Contributions of anthropogenic and natural sources of sulfur to SO2, H2SO4(g) and nanoparticle formation

D. D. Lucas, H. Akimoto

Atmos. Chem. Phys. Discuss., 7, 7679–7721, 2007
www.atmos-chem-phys-discuss.net/7/7679/2007/

Atmospheric Chemistry and Physics Discussions

Contributions of anthropogenic and natural sources of sulfur to SO_2, H_2SO_4(g) and nanoparticle formation

D. D. Lucas[1,*] **and H. Akimoto**[1]

[1]Frontier Research Center for Global Change, Japan Agency for Marine-Earth Science and Technology, 236-0001 Yokohama, Japan
[*]now at: Department of Atmospheric Sciences, Texas A & M University, College Station, TX, USA

Received: 27 April 2007 – Accepted: 16 May 2007 – Published: 4 June 2007

Correspondence to: D. D. Lucas (ddlucas@tamu.edu)

Abstract

Atmospheric nanoparticles (NPs) are important intermediates in the transition from gas-phase molecules to new aerosols that can activate into cloud droplets. Through increases in the emissions of sulfur-containing gases, human activities have likely increased the number of NPs produced in the atmosphere. To have significant impacts, however, sulfur pollution must be transported away from the surface, where NP formation is inefficient, to higher altitudes. To characterize this anthropogenic influence, tagged tracers are implemented in a global atmospheric transport model. The tagged tracers are used to track the contributions of sulfur from five sources (anthropogenic, oceanic, volcanic, aircraft, and stratospheric) to the gas-phase burdens of SO_2 and H_2SO_4(g), and the rates of forming atmospheric NPs. Because NPs may be produced by a variety of mechanisms, three different aerosol nucleation schemes (binary, ternary and ion-induced) are used in the model calculations. Of the SO_2 in the global troposphere, the tagged tracers indicate that about 69% originates from anthropogenic surface emissions, 20% from the oceans and 10% from de-gassing volcanoes. The same sources contribute about 56%, 24% and 19%, respectively, to the global tropospheric H_2SO_4(g) burden. The anthropogenic contribution for H_2SO_4(g) is reduced because anthropogenic SO_2 produces H_2SO_4(g) less efficiently than oceanic and volcanic sulfur. Regardless of the underlying nucleation assumptions, the simulations show a pronounced influence of anthropogenic sulfur on atmospheric NP formation, particularly in the Northern Hemisphere. Utilizing the tagged H_2SO_4(g) contributions, anthropogenic sulfur is estimated to account for roughly 69% of the NP formation in the Northern Hemisphere, 31% in the Southern Hemisphere and 56% across the global troposphere. In the key region of the upper troposphere, anthropogenic and oceanic sulfur both make sizeable contributions to NP formation (54% and 37%, respectively). The tagged tracer contributions suggest that human activities have probably more than doubled the NP production rate in the atmosphere from preindustrial to modern times.

ACPD

7, 7679–7721, 2007

1 Introduction

The emissions of sulfur dioxide (SO_2) to the atmosphere have increased tremendously in the last 150 years due to the production and combustion of sulfur-containing fuels (Lefohn et al., 1999; Stern, 2005). Before the industrial revolution, the main natural sources of SO_2 to the atmosphere were from volcanoes (Andres and Kasgnoc, 1998) and the oxidation of reduced sulfur compounds produced by oceanic phytoplankton (Bates et al., 1992). In the absence of explosive volcanic events, these natural sources contribute approximately 20–25 Tg S to the atmosphere per year (about 15 Tg S from the oceans and 5–10 Tg S from mildly-erupting and outgassing volcanoes). Modern-day anthropogenic emissions of SO_2, in contrast, add about 70–80 Tg S to the atmosphere per year (Olivier and Berdowski, 2001; Stern, 2005). Anthropogenic SO_2 emissions have therefore more than quadrupled the input of sulfur to the atmosphere.

One fairly well characterized consequence of this enormous anthropogenic SO_2 perturbation is an increased amount of atmospheric acidity and acid deposition (Rodhe et al., 2002). Another important, but less well known, effect is the impact on atmospheric aerosols and the climate system. Recent climate modeling simulations (Pham et al., 2005; Stier et al., 2006) are beginning to unravel how the changing sulfur emissions in the past, present and future affect aerosols and climate. New studies are also exploring the idea of intentionally injecting sulfur into the atmosphere as a way to cool climate through geo-engineering (Crutzen, 2006; Wigley, 2006).

Additional work is required in order to fully understand the complex connections between sulfur chemistry, aerosols and climate. In particular, there are still large uncertainties associated with the formation of new nanometer-sized particles (NPs) in the atmosphere (Lucas and Akimoto, 2006), the growth of NPs to cloud condensation nuclei (CCN), and the processes by which CCN influence clouds and cloud properties (Twomey, 1974). Of these many complex processes, this report focuses on atmospheric sulfur and NPs, with the goal of quantifying the contributions of anthropogenic and natural sources of sulfur to NP formation.

ACPD
7, 7679–7721, 2007

Gaseous sulfuric acid, $H_2SO_4(g)$, appears to be a requisite precursor for most of the NPs formed in the atmosphere. $H_2SO_4(g)$ is produced from SO_2 through the following oxidation sequence:

$$SO_2 \xrightarrow[HO_2]{OH,\ O_2} SO_3 \xrightarrow{H_2O} H_2SO_4. \quad \text{(R1)}$$

The resulting $H_2SO_4(g)$ has two fates. First, $H_2SO_4(g)$ is rapidly scavenged in the presence of existing atmospheric aerosols:

$$H_2SO_4 \longrightarrow \text{Existing Aerosols.} \quad \text{(R2)}$$

Second, under favorable conditions the $H_2SO_4(g)$ can combine with water vapor and possibly other stabilizing precursors such as ammonia (Napari et al., 2002), atmospheric ions (Lee et al., 2003; Kazil et al., 2006) and/or organic acids (Zhang et al., 2004) to form NPs:

$$H_2SO_4 + H_2O + \begin{bmatrix} NH_3 \\ \text{Ions} \\ \text{Organics} \\ \vdots \end{bmatrix} \longrightarrow \text{Nanoparticles.} \quad \text{(R3)}$$

It is important to point out that pathways (R2) and (R3) are coupled and competitive, whereby the presence of many existing aerosols can provide an ample surface area for $H_2SO_4(g)$ to condense upon, which can short-circuit the formation of NPs. Also note that the rate of forming NPs in pathway (R3) increases non-linearly with decreasing temperature and increasing gas-phase precursor concentrations.

Without model analysis, the aforementioned factors make it difficult to predict the impact of anthropogenic SO_2 emissions on $H_2SO_4(g)$ and NP formation. Pathway (R1) alone suggests that increased amounts of SO_2 from anthropogenic activities should

increase the levels of H_2SO_4(g) in the atmosphere. This, in turn, implies that more NPs should be formed through pathway (R3). As more NPs are formed, however, the aerosol surface area increases, which increases the loss of H_2SO_4(g) by scavenging through pathway (R2).

More importantly, anthropogenic SO_2 is emitted mainly near the surface, where it is relatively warm, and often in environments that are polluted with soot, dust and other primary and secondary aerosols. Even though the SO_2 levels associated with anthropogenic emissions are sufficient for forming NPs, the higher temperatures and aerosol loadings at the emitting sites effectively impede NP formation. Anthropogenic SO_2 must be transported away from the emitting regions, preferably to higher altitudes, to have a greater potential to perturb NP formation.

Modeling simulations are therefore needed to determine the full impacts of anthropogenic SO_2 emissions on NP formation. To elucidate these impacts, tagged tracers have been added to a global atmospheric transport model. The tagged tracers track the emissions of sulfur-containing compounds from anthropogenic and natural sources to the burdens of SO_2 and H_2SO_4(g), and the rates of forming NPs. The model and tagged tracers are described more thoroughly in the next section.

2 Description of tagged-tracer simulations

2.1 Model description

To quantify the contributions of anthropogenic and natural sources of sulfur to atmospheric NP formation, tagged sulfur tracers have been implemented and simulated using the global three-dimensional Model of Atmospheric Transport and Chemistry (MATCH). General characteristics of MATCH have been extensively described in previous reports (Rasch et al., 1997; Mahowald et al., 1997; Lawrence et al., 1999). The specific version of MATCH used for these tagged tracer simulations contains the packages for sulfur and ammonia chemistry, ion production, and aerosol nucleation that

were described in Lucas and Prinn (2003, 2005) and Lucas and Akimoto (2006). The relevant aspects of these packages for this report are briefly summarized below.

The sulfur package contains five important natural and anthropogenic sources of atmospheric sulfur. Each of these sources is described in more detail in Sect. 2.2. The sulfur package also includes gas-phase, aqueous-phase and heterogeneous kinetic pathways for producing and destroying SO_2, H_2SO_4(g) and non-sea-salt sulfate (NSS). These pathways are illustrated in Fig. 1, where each arrow in the figure represents a process that is explicitly calculated in the model.

Of the multiple pathways converting SO_2 to NSS in Fig. 1, it is important to point out that other recently developed global sulfur models (e.g. Pham et al., 1995; Rasch et al., 2000; Chin et al., 2000) contain only the gas- and aqueous-phase routes. These models assume that the gas-phase oxidation of SO_2 leads directly to NSS without going through H_2SO_4(g) as an intermediate. H_2SO_4(g) is required for forming NPs, however, so we cannot make the same assumption in our model. MATCH therefore calculates H_2SO_4(g) concentrations dynamically considering its production from gas-phase chemistry (pathway R1) and its loss from condensing on existing aerosols and forming NPs (pathways R2 and R3). Note that the current version of the model combines the NP sulfate derived from nucleation with bulk NSS. Future versions of the model will include size-resolved descriptions of NPs.

The gas-phase reaction rates (pathway R1 and other reactions such as dimethylsulfide oxidation by OH and NO_3) are calculated using a chemical mechanism and oxidant concentrations described in previous reports (Lucas and Prinn, 2003, 2005; Lucas and Akimoto, 2006). The condensation rate (pathway R2) is estimated as a first-order loss process using a Fickian diffusion formulation and prescribed aerosol surface areas. The condensation calculations are detailed in Lucas and Prinn (2005), and have been slightly altered (rates lowered by 25%) to account for overestimated aerosol surface areas in the originally prescribed fields.

The NP formation rates (pathway R3) are calculated using parameterizations for binary, ternary and ion-induced aerosol nucleation (Vehkamäki et al., 2002; Napari

ACPD
7, 7679–7721, 2007

EGU

et al., 2002; Modgil et al., 2005). These rates depend on temperature, relative humidity, atmospheric ionization, and the concentrations of H_2SO_4(g) and NH_3.

We previously evaluated these nucleation parameterizations in MATCH (Lucas and Akimoto, 2006) and found that the ternary scheme yields excessive NP formation rates throughout the troposphere. A new algorithm is not yet available for global modeling purposes, so the ternary rates have been reduced by a factor of 10^4 as a preliminary attempt to correct for their excessive values. This correction factor is estimated from the differences between nucleation rates in the real atmosphere (Kulmala et al., 2004) and those given by the ternary nucleation scheme. Note that the results in this report, which emphasize relative changes instead of absolute values, are not overly affected by the large uncertainties surrounding aerosol nucleation.

Figure 1 illustrates other pathways that can affect NP formation indirectly through the removal of SO_2. Most notable among these are dry deposition (see Lucas and Prinn, 2005) and the aqueous-phase conversion of SO_2 to NSS in cloud and rain water. These paths can greatly impact NP formation because they represent major sinks for SO_2 in the atmosphere.

For converting SO_2 to NSS in cloud and rain water, we use a modified version of the aqueous chemistry package of Barth et al. (2000). The pH calculations in this package have been modified to allow for interactions between the ammonia and sulfur cycles. The original algorithm assumed fixed ratios of ammonium and nitrate to sulfate to set the cloud water pH. We relax this assumption by calculating the pH from the balance between the cations H^+ and NH_4^+ with the anions OH^-, HCO_3^-, HSO_3^-, NO_3^- and SO_4^{2-}. The pH is then used to determine the rates of converting dissolved SO_2 to NSS by aqueous-phase reactions with dissolved H_2O_2 and O_3. Additional gas-phase concentrations required for these computations are prescribed (HNO_3, O_3 and H_2O_2 are from von Kuhlmann et al., 2003) or assumed (CO_2 is fixed at 360 parts per million).

SO_2 is also converted heterogeneously to NSS on the surface of sea-salt aerosols, as shown in Fig. 1. This pathway has been established and is estimated to be an important process in the marine boundary layer (Luria and Sievering, 1991; Sievering

ACPD
7, 7679–7721, 2007

et al., 1992). Its global impacts are less well certain, however. We have altered the treatment of this pathway used in our previous version of MATCH (Lucas and Prinn, 2005). Previously, all of the SO_2 that diffused to sea-salt aerosols was assumed to undergo scavenging, which overestimated the efficiency of this pathway. We now assume that 5% of the SO_2 that condenses on sea-salt aerosols is removed and subsequently coverted to NSS. This assumption gives first-order heterogenous conversion rates that are comparable to the value of 4×10^{-6} s^{-1} derived by Luria and Sievering (1991).

2.2 Tagged sulfur sources and their potential to form nanoparticles

Five tagged sulfur sources are implemented in MATCH. These include (1) surface emissions of SO_2 from anthropogenic activities, (2) oceanic emissions of dimethylsulfide, (3) volcanic emissions of SO_2, (4) estimates of the SO_2 emitted by aircraft, and (5) the production of SO_2 from the oxidation of carbonyl sulfide. These sources are described in more detail below and summarized in Table 1. The tagged SO_2 and H_2SO_4(g) created from these sources are individually subjected to transport, wet and dry deposition, gas- and aqueous-phase chemistry, et cetera. H_2SO_4(g) is tagged in order to calculate the contributions to NP formation and because some of the tagged sources of SO_2 are relatively more efficient at producing sulfuric acid.

The right hand side of Table 1 also indicates qualitatively the potential for the individual tagged sulfur sources to produce NPs with respect to three influential aerosol nucleation variables (sulfuric acid, temperature, and existing aerosols). In general, the greatest potential for forming NPs occurs at high H_2SO_4(g) concentrations, low temperatures and low surface areas of existing aerosols. As shown in the table and described in more detail below, none of the individual tagged sources has a high NP formation potential with respect to all three of these nucleation variables. This feature makes it difficult to predict beforehand which sulfur sources are most important to atmospheric NP formation and provides the motivation for implementing tagged tracers in our model.

ACPD
7, 7679–7721, 2007

EGU

2.2.1 Anthropogenic sulfur

The anthropogenic source of sulfur is defined using the 1995 annual average surface emissions of SO_2 in version 3.2 of the EDGAR inventory (Olivier and Berdowski, 2001). These emissions are displayed on the left hand side of Fig. 2. For convenience, the SO_2 emitted from oceanic shipping activities is included with this source. Relative to the other sources, the anthropogenic source contributes, by far, the largest amount of sulfur to the atmosphere. As a result, the oxidation of anthropogenic SO_2 can lead to very high concentrations of H_2SO_4(g), which by itself creates a high potential for forming NPs.

As shown in Fig. 2, however, anthropogenic SO_2 is primarily emitted near densely-populated regions. Such regions also exhibit relatively high loadings of existing aerosols and high air temperatures, both of which act to suppress NP formation. A recent field study in Beijing, China, for instance, found that despite the high levels of sulfur often present in Beijing's atmosphere, NP formation only occurred in air masses that were first scrubbed free of existing aerosols (Wehner et al., 2004).

The contribution of anthropogenic sulfur to NP formation therefore depends, to a large degree, on how much of this SO_2 can be transported away from the surface to other regions of the atmosphere that are colder and contain fewer existing aerosols. One particularly important region is the upper troposphere, where NP formation has been shown to be efficient (Lucas and Prinn, 2003; Lucas and Akimoto, 2006). Estimates on the amounts of surface-emitted anthropogenic SO_2 that reach the upper troposphere are not well known, but are needed to ascertain the impacts of anthropogenic sulfur on climate.

2.2.2 Oceanic sulfur

Natural oceanic emissions of dimethylsulfide (DMS) constitute the second largest source of sulfur in the model. This source is calculated in a standard manner using prescribed DMS sea surface concentrations and a sea-air flux parameterization. In the

atmosphere, DMS is chemically converted to SO_2 by gas-phase reactions with OH and NO_3. Details of these calculations, including the chemical mechanism used to oxidize DMS, are given in Lucas and Prinn (2005) and Lucas and Prinn (2003).

The oxidation of oceanic DMS can lead to high levels of SO_2 and H_2SO_4(g) in the remote marine atmosphere. H_2SO_4(g) concentrations exceeding 10^7 cm^{-3}, for example, have been reported in the remote marine boundary layer (MBL) and free troposphere. (Clarke et al., 1998a; Weber et al., 1999). As noted for the anthropogenic source of sulfur, this factor by itself creates a high potential for forming NPs. However, the MBL also experiences high temperatures and numerous sea-salt aerosols that effectively scavenge SO_2 and H_2SO_4(g). These additional factors essentially inhibit NP formation in the MBL. Indeed, field campaigns have verified that NPs are not formed under most conditions in the MBL (Clarke et al., 1998b). Though a rare MBL event has been reported (Clarke et al., 1998a), it was preceded by a precipitation-induced drop in the aerosol surface area that later allowed NP formation to occur.

Oceanic sulfur can still make significant contributions to atmospheric NP formation. DMS has a low solubility (about 10^3 times less soluble than SO_2 in liquid water at T=298 K and pH=5) and a lifetime of about 2–3 days towards loss by oxidation with OH. These characteristics imply that ample amounts of DMS can be transported above the MBL through convection. Because existing aerosols are also removed by clouds and precipitation during convective processing, convective outflow regions in the free troposphere can provide optimal conditions for producing NPs. Observations in the remote marine atmosphere are consistent with this picture (Clarke et al., 1998b), though additional measurements are needed. Further analysis is also required to determine the relative contributions of oceanic DMS and anthropogenic SO_2 to NP formation at high altitudes in the marine atmosphere.

2.2.3 Volcanic sulfur

Volcanic injections of sulfur into the atmosphere are highly variable in space and time. Andres and Kasgnoc (1998) classified volcanic SO_2 fluxes according to emissions from

"continuously" and "sporadically" erupting volcanoes. The former category represents relatively smaller fluxes from volcanoes that are in a long-term state of eruption (e.g. Kilauea, Hawaii), while the latter category is designated for large episodic injections (e.g. 10 Tg S from Mt. Pinatubo in 1991).

From a multiyear average, Andres and Kasgnoc (1998) derived a total SO_2 volcanic flux of approximately 6.7 Tg S yr^{-1} (see Table 6 therein), about 70% of which they estimated to come from continuously erupting volcanoes (see Table 1 therein). For simplicity, in these current simulations we only consider SO_2 emitted from the 49 continuously erupting volcanoes defined in Andres and Kasgnoc (1998). In future work we plan to investigate case studies of the effects of large sporadic eruptions on NP formation.

As noted in Table 1, volcanic sulfur has a varying potential to form NPs. These variations depend mainly on the altitude and magnitude of the volcanic emissions. For similar magnitudes, higher altitude volcanoes have a higher potential to form NPs because they emit SO_2 in environments with relatively lower temperatures and lower aerosol surface areas. Examples of high altitude volcanoes considered in our model include Lascar, Chile (23.37° S, 67.73° W, 5.6 km above sea level, 0.4 Tg S yr^{-1}) and Nevado del Ruiz, Columbia (4.89° N, 75.32° W, 5.3 km above sea level, 0.3 Tg S yr^{-1}).

Note that the volcanoes are smaller than the sizes of the model grid cells, and therefore not resolved. The volcanic emissions are added to the horizontal and vertical model grid cell closest to the location and summit of each volcano. These emissions are spread across the entire grid cell, resulting in lower NP formation rates than would be obtained if the volcanoes were spatially resolved.

2.2.4 Aircraft sulfur

Aircraft emissions of SO_2 are estimated from version 3.2 of the EDGAR emission inventory (Olivier and Berdowski, 2001). EDGAR does not directly provide SO_2 from aircraft, so we estimate this source using the aircraft CO_2 inventory for the year 1995. Aircraft CO_2 emissions are converted to SO_2 assuming 3.1 kg CO_2 and 0.001 kg SO_2 are released for each kg of aircraft fuel consumed (Tarrasón et al., 2004). For refer-

ence, the derived aircraft SO_2 emissions at cruise altitudes are displayed on the right hand side of Fig. 2.

As with the volcanic emissions, aircraft emit SO_2 at various altitudes. Aircraft emit SO_2 at the ground level during take-offs and landings, and at cruise altitudes of about 10–13 km during long distance flights. Near the surface, aircraft SO_2 emissions are negligible compared to other sources and occur in a relatively warm and aerosol-rich atmosphere. Accordingly, the low altitude aircraft emissions are expected to be unimportant to NP formation.

At cruise altitudes, however, aircraft emit SO_2 into a cold atmosphere nearly devoid of existing aerosols, which are ideal conditions for forming NPs. The contribution of aircraft sulfur to high altitude NP formation is difficult to predict without model analysis, however, because oceanic and anthropogenic sulfur are also transported to high altitudes. It is also important to point out that, as with the volcanic emissions, the aircraft-derived NP formation rates will likely represent lower limits because the aircraft trajectories are not spatially resolved by the model grid cells.

2.2.5 Stratospheric sulfur

Carbonyl sulfide (OCS) is photolyzed in the stratosphere to reactive sulfur. Although the absolute amount of H_2SO_4(g) that can be produced from OCS photolysis is much lower than the amount from other sources in different parts of the atmosphere, this stratospheric source occurs in a cold environment with relatively few existing aerosols. This pathway thus creates a high potential to form NPs and may help serve as a source of sulfate to replenish the stratospheric aerosol layer (Crutzen, 1976). We estimate the stratospheric source of sulfur using the total average OCS loss rate profile in Chin and Davis (1995). This profile is modulated for diurnal variations in our model, and each molecule of OCS that is photolyzed is assumed to produce one molecule of SO_2.

3 Global budgets

Before describing the results of the tagged-tracer simulations, it is useful to first compare the sulfur budgets from our model with those from other global sulfur models. The annually and globally averaged budgets for SO_2, H_2SO_4(g) and NSS are shown in Table 2. Representative ranges from other global sulfur models are shown on the right hand side of the table (taken from Tables 3 and 4 in Rasch et al., 2000). Note that many of the budget terms cannot be directly compared because the other models do not resolve the H_2SO_4(g) pathways and the sea-salt SO_2 processing pathways shown in Fig. 1.

Referring to SO_2, the table indicates that the sources from emissions and gas-phase chemistry are well within the ranges of the previous studies, as are the sinks from aqueous-phase chemistry and dry deposition. The value for the wet deposition of SO_2 appears to be low, but it is not inconsistent with other models because, as pointed out by Rasch et al. (2000), the wide range is related to the labeling of dissolved sulfur. The gas-phase chemistry sink of SO_2 also appears to be at the low end of the range from the previous studies, but those studies do not include sea-salt processing. Added together, the removal of SO_2 by gas-phase chemistry and sea-salt processing is well within the range of the gas-phase loss in the other studies. Also note that a somewhat lower SO_2 burden is predicted in our study, which is mainly due to a relatively lower rate of gas-phase production and higher rate of aqueous-phase loss. In the aqueous-chemistry calculations, higher aqueous-phase loss rates result from a combination of prescribing H_2O_2 (see Barth et al., 2000) and including NH_3, which increases cloud water pH and the solubility of SO_2.

As shown in Table 2, H_2SO_4(g) has only one source, the gas-phase production from SO_2 oxidation. Of the four H_2SO_4(g) sinks represented in the model, the condensation on existing aerosols (pathway R2) is the most rapid sulfuric acid removal process on a global basis. There are some regions in the upper troposphere where, due to the low number of existing aerosols, the nucleation sink is of equal or greater importance than

ACPD
7, 7679–7721, 2007

EGU

the condensation sink. Overall, however, it is the rapid rate of H_2SO_4(g) condensation that largely determines the low global burden of H_2SO_4(g), which we predict is about 300 times lower than the global burden of SO_2. The H_2SO_4(g) budget in the table therefore emphasizes the fact that the formation of NPs by nucleation represents just a very small fraction (less than 0.3%) of the total amount of sulfur that is cycled through the atmosphere.

Although this report does not focus on bulk sulfate aerosols, the deposition of NSS closes the atmospheric sulfur cycle. It is therefore useful to compare the NSS budget terms between models. From Table 2, the aqueous-phase source, wet and dry deposition sinks, and global burden of NSS are consistent with the other studies. The only major difference lies in the non-aqueous-phase NSS production pathways. In our study, NSS is produced from the condensation of H_2SO_4(g) and the sea-salt processing of SO_2. The other studies instead produce NSS directly from the gas-phase oxidation of SO_2. In spite of these dramatic differences, the total production and loss rates and global burdens of NSS are quite similar.

4 Contributions to sulfur gases

4.1 SO_2

The annual average column burdens (μmole S m^{-2}) and zonal vertical mole fractions (parts per trillion, ppt) of SO_2 from all of the sources (total SO_2) are shown in the upper left panels in Figs. 3 and 4. The other panels in the figures display the percent contributions of the tagged sources to the total SO_2. Table 3 also gives the total SO_2 burdens and corresponding tagged contributions in various atmospheric compartments. Note that the percent contributions are calculated relative to the sum of the tagged sources, which does not equal precisely the total SO_2 due to nonlinear processes contained in the model. However, the magnitude and spatial distribution of the sum of the tagged SO_2 tracers provides an excellent approximation to the total SO_2. For example, the

ACPD
7, 7679–7721, 2007

tagged column burdens add up to within 5% of the total SO_2 column burdens over most locations across the globe.

Not surprisingly, the figures and table indicate that the total SO_2 is comprised mainly of anthropogenic, oceanic and volcanic SO_2. The contributions from aircraft and stratospheric SO_2 are negligible, even at high altitudes where their sulfur is directly injected in the model. A more revealing feature is that the proportions of the sources in Table 1 do not match the tagged SO_2 contributions in Table 3. For instance, anthropogenic and volcanic SO_2 emissions make up about 77% and 5%, respectively, of the total amount of sulfur input into the model. The same sources account for 69% and 10% of the global SO_2 burden in Table 3. These differences occur because much of the anthropogenic SO_2 emitted at the surface is quickly removed by dry deposition. Volcanic SO_2 avoids this loss because it is injected above the surface layer.

Figures 3 and 4 also show that the oceanic and anthropogenic contributions are generally partitioned by hemisphere and land versus sea, while the volcanic contributions are large, but spatially limited. These partitioning features can potentially be exploited to help infer source-based emissions of SO_2 from remotely-sensed observations. To better illustrate this partitioning, Figs. 3 and 4 show that the anthropogenic sulfur is the overall dominant source of SO_2 throughout most of the Northern Hemisphere (NH) and over most landmasses across the globe, except for regions near volcanoes. The oceans, on the other hand, are essentially the sole source of tropospheric SO_2 from the mid-to-high latitudes in the Southern Hemisphere (SH) and the dominant source of SO_2 over tropical oceans. Oceanic sulfur even makes sizeable contributions to SO_2 over the oceans in the NH, including contributions of more than 40% over the Northeastern Pacific and the waters surrounding Greenland.

The SO_2 contributions from volcanoes are also very substantial (more than 90% in some cases), but tend to be limited to local horizontal and vertical regions. Of the many volcanoes simulated in the model, only the outgassing by Lascar, Chile (23.37° S, 67.73° W, 5592 m above sea level), makes significant contributions to SO_2 over an extended area. Lascar contributes 20–40% of the SO_2 columns over the South Atlantic

ACPD
7, 7679–7721, 2007

EGU

and 10–20% across the Southern Indian Ocean. The extended volcanic SO_2 over the South Atlantic leads to the situation where there are nearly equal contributions from the volcanic, anthropogenic and oceanic sources (about 30% each) in that region.

As mentioned in Sect. 2.2.1, the amount of anthropogenic SO_2 that reaches the upper troposphere remains poorly quantified, but is important for understanding anthropogenic perturbations to the sulfur cycle. Thornton et al. (1997) estimated this quantity using high-altitude SO_2 and DMS measurements over the central and western Pacific Ocean during two periods, September–October 1991 and February–March 1994. They found higher SO_2 levels during the earlier period (about 40–200 ppt compared to 10–50 ppt), which they attributed to volcanic activity. On the basis of their DMS measurements, Thornton et al. (1997) concluded that the oceanic source accounted for less than 1% of the SO_2 in the western Pacific upper troposphere in 1991 and less than 10% in 1994.

The estimates of the oceanic contributions from Thornton et al. (1997) are clearly lower than our results in Table 3 and Figs. 3 and 4. This is an important discrepancy to resolve because lower oceanic contributions imply stronger perturbations of anthropogenic activities on the sulfur cycle. The recent study by Notholt et al. (2005), for example, may have overestimated the impacts of anthropogenic Asian SO_2 emissions on stratospheric humidity because they used the low value for the oceanic contribution (less than 10%) of Thornton et al. (1997) in their analysis.

To help clear up this discrepancy, Fig. 5 displays the monthly average mole fractions and percent oceanic contributions of SO_2 at high altitudes over the western Pacific for February and September. The simulated mole fractions in our model are consistent with the high altitude measurements of Thornton et al. (1997), giving levels of roughly 10–50 ppt during February and 50–200 ppt during September. Thornton et al. (1997) attributed the differences between the two periods to volcanic activity. Because volcanic and anthropogenic SO_2 emissions do not vary with time in our model, our simulations show that seasonal differences in atmospheric transport and convection can also greatly affect SO_2 at high altitudes in this region.

Moreover, the oceanic contributions in Fig. 5 suggest that DMS accounts for more than 30% of the high-altitude SO_2 across most of the western Pacific in February and, except for continental areas near Asia and Russia, more than 10% during September. The oceanic contributions estimated by Thornton et al. (1997) are likely too low because their analysis did not fully account for SO_2 which is formed from DMS in other locations in the atmosphere and later transported to the upper troposphere. Without a doubt, the oceanic SO_2 contributions shown in Fig. 5 vary dramtically with season and location, so we do not recommend the use of small and constant oceanic contributions, as in Notholt et al. (2005).

4.2 H_2SO_4(g)

The annual average column burdens (nmole S m^{-2}) and zonal vertical number concentrations (molecules cm^{-3}) of H_2SO_4(g) are shown in Figs. 6 and 7. The upper left panels in the figures display the total H_2SO_4(g) from all of the sources, while the other panels give the percent contributions to the total H_2SO_4(g) from the tagged tracers. Table 3 also reports the total burdens and tagged contributions in various atmospheric compartments. Note that the H_2SO_4(g) column burdens are displayed using a scale that is a thousand times smaller than for SO_2.

Also, as before, the percentages are calculated relative to the sum of the tagged H_2SO_4(g) tracers. Like SO_2, this sum provides an excellent estimate of the total H_2SO_4(g). At all locations throughout Figs. 6 and 7, the tagged sum falls within 10% of the total H_2SO_4(g). Given that the loss of H_2SO_4(g) by NP formation is highly nonlinear, it may seem surprising that the tagged sum nearly equals the total H_2SO_4(g). Recall, however, that the major sink for H_2SO_4(g) is condensation on existing aerosols (see Table 2), which is a linear removal process. The tagged tracers can therefore be used to quantify the source-based sulfur contributions to H_2SO_4(g).

The profile of the total H_2SO_4(g) displayed in Fig. 7 differs slightly from our previous profile in Lucas and Akimoto (2006) (Fig. 1 therein). Excessive ternary nucleation rates in the prior version of the model caused rapid H_2SO_4(g) removal in the upper

tropical troposphere. This, in turn, led to a region of depleted H_2SO_4(g) concentrations that were below 10^4 cm^{-3}. For the current simulations, the ternary nucleation rates have been reduced (see Sect. 2.1), which has increased the H_2SO_4(g) in the upper tropical troposphere to levels believed to be more consistent with measurements (10^5 to 10^6 cm^{-3}).

Along with water vapor and OH radicals, pathway (R1) shows that SO_2 is a necessary precursor for H_2SO_4(g). This implies that the atmospheric distributions and source-based contributions between SO_2 and H_2SO_4(g) should have many features in common. Comparing Figs. 3 and 4 with Figs. 6 and 7 shows that this is indeed the case. The total SO_2 and total H_2SO_4(g) in these figures are both concentrated near populated regions, relatively larger over land than sea, and present in larger quantities in the NH than the SH.

In terms of the tagged tracers, the anthropogenic contributions account for nearly all of the total column burdens of both SO_2 and H_2SO_4(g) above North America and Eurasia. Moreover, the oceanic contributions comprise more than 70% of the total amounts of both species across most of the SH. The strong similarities between SO_2 and H_2SO_4(g) even hold in regions where there are comparable contributions from the different tagged sources. For example, volcanic, oceanic and anthropogenic sulfur each make up about 30% of the column burdens of SO_2 and H_2SO_4(g) over the South Atlantic (Fig. 6), while oceanic and anthropogenic sulfur account for about 50% of both species in the upper tropical troposphere (Fig. 7).

Because the production of H_2SO_4(g) from SO_2 also depends directly on OH radicals, the H_2SO_4(g) and SO_2 atmospheric distributions differ in important ways. These OH-related differences are most apparent in the zonal vertical profiles in Figs. 4 and 7. The largest SO_2 concentrations in Fig. 4 are located between 25° N and 60° N above the anthropogenic-emitting regions in the NH. Figure 7, in contrast, shows high concentrations of H_2SO_4(g) across the lower and middle latitudes of both hemispheres (30°S to 50°N). In the conversion of SO_2 to H_2SO_4(g), the latitudes of the peak values have therefore shifted from the extratropics to the tropics. This shift results from the photo-

chemical production of OH, which maximizes in the tropics (see Fig. 12 in Lawrence et al., 1999).

Besides the OH-related differences, the rapid loss of sulfuric acid on existing aerosols leads to additional differences between the atmospheric distributions of SO_2 and H_2SO_4(g). Most noticeably, the largest total H_2SO_4(g) column burdens in Fig. 6 are caused by volcanic SO_2 emissions (e.g. near Mt. Etna, Italy), whereas the largest total SO_2 column burdens in Fig. 3 are associated with anthropogenic emissions over Asia. Similarly, Fig. 4 indicates that the largest SO_2 concentrations are present near the surface, while Fig. 7 shows that the peak H_2SO_4(g) concentrations occur well above the surface. These differences arise for two reasons related to existing aerosols. First, anthropogenic SO_2 is emitted near the surface, where any H_2SO_4(g) that is subsequently formed is rapidly scavenged by existing aerosols. Second, volcanoes emit SO_2 at higher altitudes, where there are fewer existing aerosols and, hence, a smaller sink for H_2SO_4(g).

On a related note, H_2SO_4(g) has a short atmospheric lifetime due to its rapid scavenging by existing aerosols. SO_2, on the other hand, has a much longer lifetime, which makes it susceptible to changes from atmospheric transport. Through transport, SO_2 can be carried to/from regions of the atmosphere where dry deposition and aqueous-phase removal are more/less effective. Even though a large portion of the SO_2 emitted in a polluted region is lost by dry deposition, for example, a significant amount of the remaining SO_2 can still be lofted to high altitudes through convection.

The longer lifetime of SO_2, along with the spatially heterogeneous SO_2 sources and sinks, implies that on a large scale, the tagged-tracer contributions are not preserved as SO_2 is converted to H_2SO_4(g). One illustration of this is shown in Table 3. The anthropogenic, oceanic and volcanic contributions to the global burden of SO_2 are 69%, 20% and 10%, respectively. The same contributions for H_2SO_4(g) are 56%, 24% and 19%. The differences between these sets of contributions indicates that oceanic and volcanic sulfur are converted to H_2SO_4(g) more efficiently than anthropogenic sulfur.

To better illustrate the conversion differences, the SO_2 to H_2SO_4(g) conversion effi-

ciency is displayed in Fig. 8. The conversion efficiency, which is independent of SO_2, is defined as the ratio of the loss of SO_2 by gas-phase chemistry to the net loss of SO_2 by gas- and aqueous-phase oxidation, sea-salt processing, and wet and dry deposition. Figure 8 shows, for instance, that the SO_2 over Northern Africa is converted to H_2SO_4(g) with efficiencies approaching 60%. The large efficiencies is this particular region are due to dry conditions and reduced levels of aqueous-phase removal. In terms of anthropogenic SO_2, comparing Fig. 8 with Fig. 2 clearly shows that the regions with the largest anthropogenic emissions, namely Europe, Western China and the Eastern United States, are also the regions with the lowest SO_2 to H_2SO_4(g) conversion efficiencies. The exceedingly low efficiencies in these regions are a consequence of the rapid removal of SO_2 by dry deposition and aqueous-phase chemistry. Figure 8 therefore shows that the full impact of anthropogenic activities on NP formation, as analyzed in the next section, is somewhat diminished because the anthropogenic SO_2 emissions are co-located with the major SO_2 sinks.

5 Contributions to nanoparticle formation

The annual and zonal average rates of producing atmospheric nanoparticles by the binary, ternary and ion-induced nucleation parameterizations are shown in Figs. 9 to 11. The upper left panels, as before, show the NP formation rates considering all of the sources of sulfur (total nucleation). The other panels show the rates from the individual tagged tracers. Instead of displaying the tagged contributions as relative percentages of the total, as in the previous figures for SO_2 and H_2SO_4(g), they are shown as absolute rates. They are shown in this manner because NP formation is a highly nonlinear process, which implies that the sum of the rates from the tagged tracers is a poor approximation to the rate of forming NPs from the total amount of sulfur. That is, $J_{total} \neq J_{anthropogenic} + J_{oceanic} + J_{volcanic} + J_{aircraft} + J_{stratospheric}$, where J denotes an NP formation rate. To illustrate the degree of nonlinearity, the binary nucleation rate has a cubic to quartic dependence on the H_2SO_4(g) concentration at upper tropospheric

conditions (Vehkamäki et al., 2002).

The total NP formation rates in different atmospheric compartments are also shown in Table 4. Volume-weighted values are displayed in the table so that the NP formation rates in different portions of the atmosphere can be compared to one another. Non-weighted rates give the number of new aerosols formed per unit volume per unit time (i.e. in units of cm^{-3} s^{-1}), but the atmospheric compartments in the table encompass different volumes. The rates are therefore weighted by the ratio of the volume of the compartment to the total volume. This weighting scheme yields values that are identical to dividing the number of new particles formed in the compartment by the number formed in the whole troposphere using a rate of $1\,cm^{-3}\,s^{-1}$. A rate of $1\,cm^{-3}\,s^{-1}$ is generally considered to indicate significant new particle production, so compartments with weighted values larger than unity represent important regions of NP formation.

These three nucleation schemes were evaluated in our previous report (Lucas and Akimoto, 2006). In that report, the largest NP formation rates were calculated using the ternary nucleation parameterization, followed by binary and ion-induced nucleation, respectively. Because of the correction factor that was applied to ternary nucleation (see Sect. 2.1), the largest rates in this current report are now computed by binary nucleation. The changes between these reports are immaterial, however, due to the enormous uncertainties surrounding the individual aerosol nucleation mechanisms and the inability of atmospheric observations to distinguish among them.

The remainder of this report therefore ignores the order and absolute values of the NP formation rates computed by the three nucleation mechanisms. In spite of this limitation, important conclusions can still be drawn by examining relative features that exist in all three nucleation schemes. One such feature is that NPs are formed less rapidly near the surface than at higher altitudes because of the warmer conditions and more existing aerosols present at the surface. Another such feature is that the NP formation rates are relatively larger in the NH than the SH, which points to an influence of anthropogenic activities on NP formation.

Even though the percent contributions to the NP formation rates are not displayed,

Figs. 9 to 11 still give a strong qualitative indication of the influence of the various sources of sulfur on NP formation. The figures show, for instance, that atmospheric NPs are formed primarily from anthropogenic, oceanic and volcanic sulfur. Of these, our simulations indicate that anthropogenic sulfur is the dominant source of new NPs formed in the troposphere, though the contributions from volcanic and oceanic sulfur cannot be neglected.

In order to better understand the impacts of human activities on the climate system, it is important to quantify the number of new atmospheric NPs that can be formed from anthropogenic SO_2. Sulfur emissions to the atmosphere increased by about a factor of four from preindustrial to modern times (Lefohn et al., 1999; Stern, 2005), but the anthropogenic nucleation rates in Figs. 9 to 11 are not four times higher than the natural sulfur (oceanic + volcanic) nucleation rates.

To quantify this anthropogenic perturbation, we argue that since $H_2SO_4(g)$ is a main limiting factor in NP production, the tagged $H_2SO_4(g)$ tracer contributions can be used to estimate the relative number of new NPs produced from anthropogenic SO_2. Our rationale is based on the short atmospheric lifetime of $H_2SO_4(g)$. Any sulfuric acid molecules that are produced are lost almost immediately, so nucleation is localized and the proportions of the tagged $H_2SO_4(g)$ tracers are approximately preserved as NPs are formed. Recall that the tagged-tracer contributions are not conserved as SO_2 is converted to $H_2SO_4(g)$ because SO_2 has a longer lifetime and is therefore heavily influenced by atmospheric transport.

To show that the proportions of the tagged $H_2SO_4(g)$ tracers are preserved during NP formation, assume that $J \propto [H_2SO_4]^3$ and $[H_2SO_4]=[H_2SO_4]_A+[H_2SO_4]_B$, where J is the total nucleation rate, $[H_2SO_4]$ is the total sulfuric acid concentration, and $[H_2SO_4]_A$ and $[H_2SO_4]_B$ represent sulfuric acid from different sources. Expanding the total nucleation rate gives:

$$J \propto [H_2SO_4]_A^3 + 3[H_2SO_4]_A^2[H_2SO_4]_B + 3[H_2SO_4]_A[H_2SO_4]_B^2 + [H_2SO_4]_B^3.$$

Assuming that the cross terms are partitioned by their polynomial orders, the contribution of source A to the total nucleation, denoted J_A, is given by:

$$J_A = [H_2SO_4]_A^3 + 2[H_2SO_4]_A^2[H_2SO_4]_B + [H_2SO_4]_A[H_2SO_4]_B^2 = [H_2SO_4]_A([H_2SO_4]_A + [H_2SO_4]_B)^2.$$

Note that because of the nonlinearity in nucleation, J_A does not equal $J([H_2SO_4]_A)$. The fractional contribution of source A to the total nucleation is then:

$$\frac{J_A}{J} = \frac{[H_2SO_4]_A([H_2SO_4]_A + [H_2SO_4]_B)^2}{([H_2SO_4]_A + [H_2SO_4]_B)^3} = \frac{[H_2SO_4]_A}{[H_2SO_4]_A + [H_2SO_4]_B}.$$

The right hand side represents the fraction of source A in the total sulfuric acid, thus the proportions of the tagged H_2SO_4(g) tracers are preserved during NP formation.

On the basis of the above arguments, the H_2SO_4(g) contributions in Table 3 suggest that more than 50% of the NPs that are formed in the modern global troposphere originate from anthropogenic SO_2. In the NH and SH, the table values translate into anthropogenic SO_2 contributions of about 69% and 31%, respectively. We stress that these estimates are relative values, are irrespective of the aerosol nucleation mechanisms, and are for the 1995 base year of anthropogenic emissions. In order to calculate definitive numbers of NPs formed from anthropogenic SO_2, the specific nucleation mechanisms must be better constrained.

From preindustrial to modern times, we also estimate that the production rate of NPs in the atmosphere has likely more than doubled due to anthropogenic activities tied to SO_2. This estimate is based on using the 50% contribution as a lower bound and considering nonlinearities in the calculations. That is, doubling the sulfuric acid concentration normally more than doubles the NP formation rate due to the nonlinearity

ACPD
7, 7679–7721, 2007

EGU

in NP formation. This is only a rough estimate, however, because the aerosol surface areas used in the scavenging calculations (pathway R2) are not representative of preindustrial conditions. Nonetheless, we believe that this is still a reasonable estimate because the H_2SO_4(g) formed in the preindustrial atmosphere (i.e. from the oceanic and volcanic sulfur sources) is preferentially scavenged by natural aerosol components (e.g. mineral dust and sea salt) that are adequately represented in our model.

6 Summary

Atmospheric nanoparticles lie at the interface between the sulfur-containing gases SO_2 and H_2SO_4(g) and new aerosols that can grow into cloud condensation nuclei. Anthropogenic activities have increased the SO_2 levels in the atmosphere, but little is known about the subsequent impacts on nanoparticle formation. To address this issue, tagged sulfur tracers have been included in the 3-D global tropospheric MATCH model. Tracers were tagged according to sulfur emissions from anthropogenic, oceanic, volcanic, aircraft and stratospheric sources. The source-based contributions to SO_2, H_2SO_4(g), and nanoparticle formation were then quantified using the tagged tracers.

The simulations reveal sharp spatial differences in the source-based contributions to the burdens of SO_2 and H_2SO_4(g). Over the Northern and Southern Hemispheres, respectively, these two gases originate mainly from anthropogenic and oceanic sulfur. Likewise, there is a prominent contrast between land and sea, with anthropogenic sulfur dominating over land and oceanic sulfur dominating over the oceans. Significant contributions are also estimated from degassing volcanoes, though these contributions are confined to fairly localized areas. In the global troposphere, anthropogenic, oceanic and volcanic sources of sulfur are estimated to account for 69%, 20% and 10% of the SO_2, respectively. For H_2SO_4(g) the same sources contribute approximately 56%, 24% and 19%.

Even though anthropogenic SO_2 is emitted primarily at the surface and nanoparticles are formed away from the surface, this study shows that anthropogenic activities have

very substantial impacts on nanoparticle formation. This finding occurs irrespective of the exact mechanisms behind aerosol nucleation. Of the three nucleation schemes tested in the simulations, all indicate that anthropogenic SO_2 is the dominant source of nanoparticles. The tagged-tracer contributions suggest that approximately 50% of the nanoparticles formed in the troposphere are from anthropogenic SO_2. This then implies that anthropogenic activities have probably more than doubled the production rate of nanoparticles in the troposphere from preindustrial to modern times. To better ascertain the true impacts of these anthropogenic SO_2 changes on climate, future studies will require connecting the nanoparticles to larger-sized condensation nuclei and cloud condensation nuclei.

References

Andres, R. J. and Kasgnoc, A. D.: A time-averaged inventory of subaerial volcanic sulfur emissions, J. Geophys. Res., 103, 25 251–25 261, 1998. 7681, 7688, 7689

Barth, M. C., Rasch, P. J., Kiehl, J. T., Benkovitz, C. M., and Schwartz, S. E.: Sulfur chemistry in the National Center for Atmospheric Research Community Climate Model: Description, evaluation, features, and sensitivity to aqueous chemistry, J. Geophys. Res., 105, 1387–1415, doi:10.1029/1999JD900773, 2000. 7685, 7691

Bates, T. S., Lamb, B. K., Guenther, A., Dignon, J., and Stoiber, R. E.: Sulfur emissions to the atmosphere from natural sources, J. Atmos. Chem., 14, 315–337, 1992. 7681

Chin, M. and Davis, D. D.: A reanalysis of carbonyl sulfide as a source of stratospheric background sulfur aerosol, J. Geophys. Res., 100, 8993–9005, 1995. 7690

Chin, M., Rood, R. B., Lin, S. J., Müller, J. F., and Thompson, A. M.: Atmospheric sulfur cycle simulated in the global model GOCART: Model description and global properties, J. Geophys. Res., 105, 24 671–24 687, doi:10.1029/2000JD900384, 2000. 7684

Clarke, A. D., Davis, D., Kapustin, V. N., Eisele, F., Chen, G., Paluch, I., Lenschow, D., Bandy, A. R., Thorton, D., Moore, K., Mualdin, L., Tanner, D., Litchy, M., Carroll, M. A., Collins, J., and Albercook, G.: Particle nucleation in the tropical marine boundary layer and its coupling to marine sulfur sources, Science, 282, 89–92, 1998a. 7688

Clarke, A. D., Varner, J. L., Eisele, F., Mauldin, R. L., Tanner, D., and Litchy, M.: Particle

production in the remote marine atmosphere: Cloud outflow and subsidence during ACE 1, J. Geophys. Res., 103, 16 397–16 409, 1998b. 7688
Crutzen, P. J.: The possible importance of COS for the sulfate layer of the stratosphere, Geophys. Res. Lett., 3, 73–76, 1976. 7690
Crutzen, P. J.: Albedo enhancement by stratospheric sulfur injections: A contribution to resolve a policy dilemma?, Climatic Change, 77, 211–219, doi:10.1007/s10584-006-9101-y, 2006. 7681
Kazil, J., Lovejoy, E. R., Barth, M. C., and O'Brien, K.: Aerosol nucleation over oceans and the role of galactic cosmic rays, Atmos. Chem. Phys., 6, 4905–4924, 2006, http://www.atmos-chem-phys.net/6/4905/2006/. 7682
Kulmala, M., Vehkamäki, H., Petäjä, T., Dal Maso, M., Lauri, A., Kerminen, V.-M., Birmili, W., and McMurry, P. H.: Formation and growth rates of ultrafine atmospheric particles: A review of observations, J. Aerosol Sci., 35, 143–176, 2004. 7685
Lawrence, M. G., Crutzen, P. J., Rasch, P. J., Eaton, B. E., and Mahowald, N. M.: A model For studies of tropospheric photochemistry: Description, global distributions, and evaluation, J. Geophys. Res., 104, 26 245–26 277, 1999. 7683, 7697
Lee, S.-H., Reeves, J. M., Wilson, J. C., Hunton, D. E., Viggiano, A. A., Miller, T. M., Ballenthin, J. O., and Lait, L. R.: Particle formation by ion nucleation in the upper troposphere and lower stratosphere, Science, 301, 1886–1889, 2003. 7682
Lefohn, A. S., Husar, J. D., and Husar, R. B.: Estimating historical anthropogenic global sulfur emission patterns for the period 1850–1990, Atmos. Environ., 33, 3435–3444, 1999. 7681, 7700
Lucas, D. D. and Akimoto, H.: Evaluating aerosol nucleation parameterizations in a global atmospheric model, Geophys. Res. Lett., 33, L10 808, doi:10.1029/2006GL025672, 2006. 7681, 7684, 7685, 7687, 7695, 7699
Lucas, D. D. and Prinn, R. G.: Tropospheric distributions of sulfuric acid-water vapor aerosol nucleation rates from dimethylsulfide oxidation, Geophys. Res. Lett., 30, 2136, doi:10.1029/2003GL018370, 2003. 7684, 7687, 7688
Lucas, D. D. and Prinn, R. G.: Sensitivities of gas-phase dimethylsulfide oxidation products to the assumed mechanisms in a chemical transport model, J. Geophys. Res., 110, D21 312, doi:10.1029/2004JD005386, 2005. 7684, 7685, 7686, 7688
Luria, M. and Sievering, H.: Heterogeneous and homogeneous oxidation of SO_2 in the remote marine atmosphere, Atmos. Environ. Part A, 25, 1489–1496, 1991. 7685, 7686

Mahowald, N., Rasch, P., Eaton, B., Whittlestone, S., and Prinn, R.: Transport of ^{222} Radon to the remote troposphere using the Model of Atmospheric Transport and Chemistry and assimilated winds from ECMWF and the National Center for Environmental Prediction/NCAR, J. Geophys. Res., 102, 28 139–28 151, 1997. 7683

Modgil, M. S., Kumar, S., Tripathi, S. N., and Lovejoy, E. R.: A parameterization of ion-induced nucleation of sulphuric acid and water for atmospheric conditions, J. Geophys. Res., 110, D19205, doi:10.1029/2004JD005475, 2005. 7685

Napari, I., Noppel, M., Vehkamäki, H., and Kulmala, M.: Parameterization of ternary nucleation rates for H_2SO_4-NH_3-H_2O vapors, J. Geophys. Res., 107, 4381, doi:10.1029/2002JD002132, 2002. 7682, 7684

Notholt, J., Luo, B. P., Fueglistaler, S., Weisenstein, D., Rex, M., Lawrence, M. G., Bingemer, H., Wohltmann, I., Corti, T., Warneke, T., von Kuhlmann, R., and Peter, T.: Influence of tropospheric SO_2 emissions on particle formation and the stratospheric humidity, Geophys. Res. Lett., 32, doi:10.1029/2004GL022159, 2005. 7694, 7695

Olivier, J. and Berdowski, J.: Global emissions sources and sinks, in: The Climate System, edited by: Berdowski, J., Guicherit, R., and Heij, B., pp. 33–77, A. A. Balkema Publishers, Swets and Zeitlinger Publishers, Lisse, The Netherlands, 2001. 7681, 7687, 7689

Pham, M., Müller, J., Brasseur, G., Granier, C., and Mégie, G.: A three dimensional study of the tropospheric sulfur cycle, J. Geophys. Res., 100, 26 061–26 092, 1995. 7684

Pham, M., Boucher, O., and Hauglustaine, D.: Changes in atmospheric sulfur burdens and concentrations and resulting radiative forcings under IPCC SRES emission scenarios for 1990–2100, J. Geophys. Res., 110, D06112, doi:10.1029/2004JD005125, 2005. 7681

Rasch, P., Mahowald, N., and Eaton, B.: Representations of transport, convection, and the hydrologic cycle in chemical transport models: Implications for the modeling of short-lived and soluble species, J. Geophys. Res., 102, 28 127–28 138, 1997. 7683

Rasch, P. J., Barth, M. C., Kiehl, J. T., Schwartz, S. E., and Benkovitz, C. M.: A Description of the global sulfur cycle and its controlling processes in the National Center for Atmospheric Research Community Climate Model, Version 3, J. Geophys. Res., 105, 1367–1385, doi:10.1029/1999JD900777, 2000. 7684, 7691, 7708

Rodhe, H., Dentener, F., and Schulz, M.: The global distribution of acidifying wet deposition, Environ. Sci. Technol., 36, 4382–4388, 2002. 7681

Sievering, H., Boatman, J., Gorman, E., Kim, Y., Anderson, L., Ennis, G., Luria, M., and Pandis, S.: Removal of sulphur from the marine boundary layer by ozone oxidation in sea-salt

aerosols, Nature, 360, 571–573, 1992. 7685
Stern, D. I.: Global sulfur emissions from 1850 to 2000, Chemosphere, 58, 163–175, doi: 10.1016/j.chemosphere.2004.08.022, 2005. 7681, 7700
Stier, P., Feichter, J., Roeckner, E., Kloster, S., and Esch, M.: The evolution of the global aerosol system in a transient climate simulation from 1860 to 2100, Atmos. Chem. Phys., 6, 3059–3076, 2006, http://www.atmos-chem-phys.net/6/3059/2006/. 7681
Tarrasón, L., Jonson, J. E., Berntsen, T. K., and Rypdal, K.: Study on air quality impacts of non-LTO emissions from aviation, Tech. Rep. 3, Final report to the European Commission under contract B4-3040/2002/343093/MAR/C1, 2004. 7689
Thornton, D. C., Bandy, A. R., Blomquist, B. W., Bradshaw, J. D., and Blake, D. R.: Vertical transport of sulfur dioxide and dimethyl sulfide in deep convection and its role in new particle formation, J. Geophys. Res., 102, 28 501–28 510, doi:10.1029/97JD01647, 1997. 7694, 7695
Twomey, S.: Pollution and the planetary albedo, Atmos. Environ., 8, 1251–1256, 1974. 7681
Vehkamäki, H., Kulmala, M., Napari, I., Lehtinen, K. E., Timmreck, C., Noppel, M., and Laaksonen, A.: An improved parameterization for sulfuric acid-water nucleation rates for tropospheric and stratospheric conditions, J. Geophys. Res., 107, 4622, doi:10.1029/2002JD002184, 2002. 7684, 7699
von Kuhlmann, R., Lawrence, M., Crutzen, P., and Rasch, P.: A model for studies of tropospheric ozone and nonmethane hydrocarbons: Model description and ozone results, J. Geophys. Res., 108, 4294, doi:10.1029/2002JD002893, 2003. 7685
Weber, R. J., McMurry, P. H., Mauldin III, R. L., Tanner, D. J., Eisele, F. L., Clarke, A. D., and Kapustin, V. N.: New particle formation in the remote troposphere: A comparison of observations at various sites, Geophys. Res. Lett., 26, 307–310, 1999. 7688
Wehner, B., Wiedensohler, A., Tuch, T. M., Wu, Z. J., Slanina, J., and Kiang, C. S.: Variability of the aerosol number size distribution in Beijing, China: New particle formation, dust storms, and high continental background, Geophys. Res. Lett., 31, doi:10.1029/2004GL021596, L22108, 2004. 7687
Wigley, T. M. L.: A combined mitigation/geoengineering approach to climate stabilization, Science, doi:10.1126/science.1131728, 2006. 7681
Zhang, R., Suh, I., Zhao, J., Zhang, D., Fortner, E. C., Tie, X., Molina, L. T., and Molina, M. J.: Atmospheric new particle formation enhanced by organic acids, Science, 304, 1487–1490, 2004. 7682

Table 1. Tagged sources of sulfur considered in the model, and their annual source amounts and potential to form nanoparticles with respect to three variables. A high potential to form NPs occurs at high H_2SO_4(g) concentrations, low temperatures (T), and low levels of existing aerosols. The potential to form NPs refers to the conditions at the location of the source in the model. Refer to Sect. 2.2 for further discussion.

Tagged source	Species	Amount	Potential to form NPs with respect to:		
		(Tg S yr^{-1})	H_2SO_4(g)	T	Existing aerosols
Anthropogenic	SO_2	76	high	low	low
Oceanic	DMS	17	high	low	low
Volcanic	SO_2	5	low–high	low–high	low–high
Aircraft	SO_2	0.1	low	low–high	low–high
Stratospheric	OCS	0.02	low	high	high

Table 2. The annual-global average budgets of SO_2, H_2SO_4(g) and Non-sea-salt sulfate (NSS). Ranges for SO_2 and NSS from other studies are displayed on the right hand side (from Tables 3 and 4 in Rasch et al., 2000).

	This study			Other studies	
	SO_2	H_2SO_4(g)	NSS	SO_2	NSS
Sources (Tg S/yr)					
emissions	81	–	–	65–92	0–4
gas-phase	16	5	–	14–22	6–17
aqueous-phase	–	–	53	–	34–56
condensation	–	–	5	–	–
nucleation	–	–	<1	–	–
sea-salt path	–	–	3	–	–
Sinks (Tg S/yr)					
gas-phase	5	–	–	6–17	–
aqueous-phase	53	–	–	34–55	–
condensation	–	5	–	–	–
sea-salt path	3	–	–	–	–
nucleation	–	<1	–	–	–
dry deposition	36	<1	12	22–55	4–18
wet deposition	<1	<1	50	0–20	44–54
Burdens (Tg S)	0.2	0.0008	0.6	0.2–0.6	0.5–1.1

Table 3. Annual average SO_2 and H_2SO_4(g) burdens and tagged-tracer percent contributions in different atmospheric compartments. Table abbreviations are defined as follows: NH and SH = Northern and Southern Hemisphere, respectively. T, LT, MT, and UT = full, lower, middle and upper troposphere, respectively. Vertical compartments are defined as T≈1000–89 hPa, LT≈1000–724 hPa, MT≈724–403 hPa, and UT≈403–89 hPa.

	Global				NH				SH			
	T	LT	MT	UT	T	LT	MT	UT	T	LT	MT	UT
Burdens												
SO_2 (Gg S)	214	138	35	41	160	112	23	26	54	26	13	15
H_2SO_4(g) (Mg S)	758	327	275	156	494	212	182	100	263	114	93	56
SO_2 contributions (%)												
Anthropogenic	69	78	50	52	80	87	63	64	36	42	28	31
Oceanic	20	13	29	39	11	6	17	29	47	40	49	56
Volcanic	10	9	20	6	8	7	18	3	17	18	23	11
Aircraft	1	0	1	2	1	0	2	3	0	0	0	0
Stratospheric	0	0	0	1	0	0	0	1	0	0	0	1
H_2SO_4(g) contributions (%)												
Anthropogenic	56	57	56	54	69	72	68	65	31	30	32	33
Oceanic	24	18	23	37	15	10	13	27	41	32	44	56
Volcanic	19	25	20	6	15	17	18	3	27	38	23	10
Aircraft	1	0	1	2	1	0	1	3	0	0	0	0
Stratospheric	0	0	0	1	0	0	0	1	0	0	0	1

Table 4. Annual average nanoparticle formation rates in different atmospheric compartments by three aerosol nucleation mechanisms. The rates are weighted by the ratio of the volume of the compartment to the total volume as described in Sect. 5. Refer to Table 3 for table abbreviations. Also note that the rates from ion-induced nucleation have been increased by a factor of 100.

	Global				NH				SH			
	T	LT	MT	UT	T	LT	MT	UT	T	LT	MT	UT
NP formation rates (cm^{-3} s^{-1})												
Binary	16.4	0.1	0.6	15.7	15.4	<0.1	0.5	14.9	1.0	0.1	<0.1	0.9
Ternary	3.0	1.0	1.3	0.7	2.1	0.8	0.9	0.4	1.0	0.3	0.4	0.3
Ion ($\times 10^2$)	3.1	<0.1	0.4	2.7	2.6	<0.1	0.3	2.3	0.5	<0.1	0.1	0.4

ACPD
7, 7679–7721, 2007

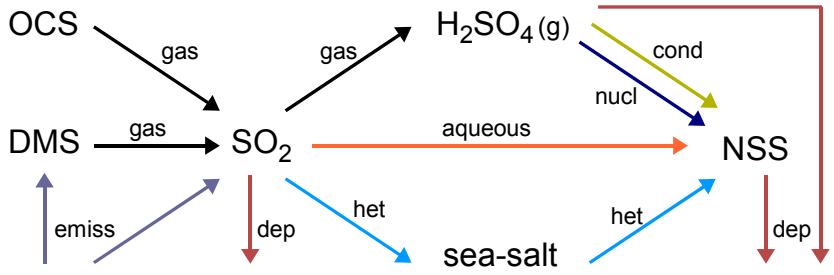

Fig. 1. The chemical and physical processes represented in the model by which SO_2 is produced and converted to H_2SO_4(g) and non-sea-salt sulfate (NSS). The pathways are labeled as follows: *emiss* = emissions; *gas* = gas-phase chemistry; *aqueous* = aqueous-phase chemistry in cloud and rain water; *het* = heterogeneous conversion on sea salt; *cond* = condensation on existing aerosols; *nucl* = nucleation of nanoparticles; and *dep* = wet and dry deposition. Refer to Table 2 for the budgets associated with these pathways.

ACPD
7, 7679–7721, 2007

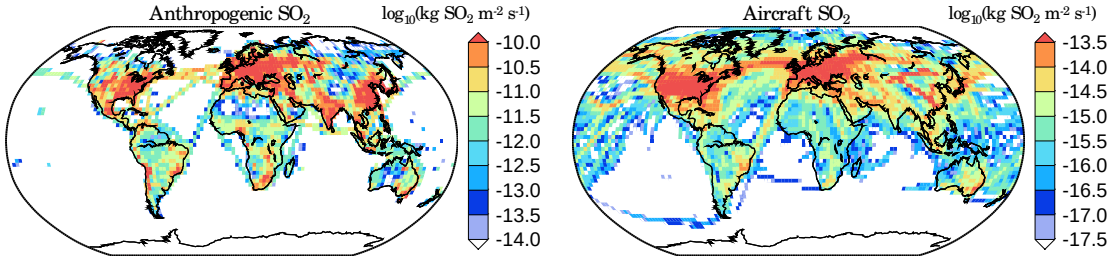

Fig. 2. Annual average SO_2 emissions from anthropogenic activities at the surface (left panel) and aircraft at a sample cruise altitude level in the upper troposphere (right panel). The sample cruise altitude corresponds to the approximate model level of 284–341 hPa.

ACPD
7, 7679–7721, 2007

EGU

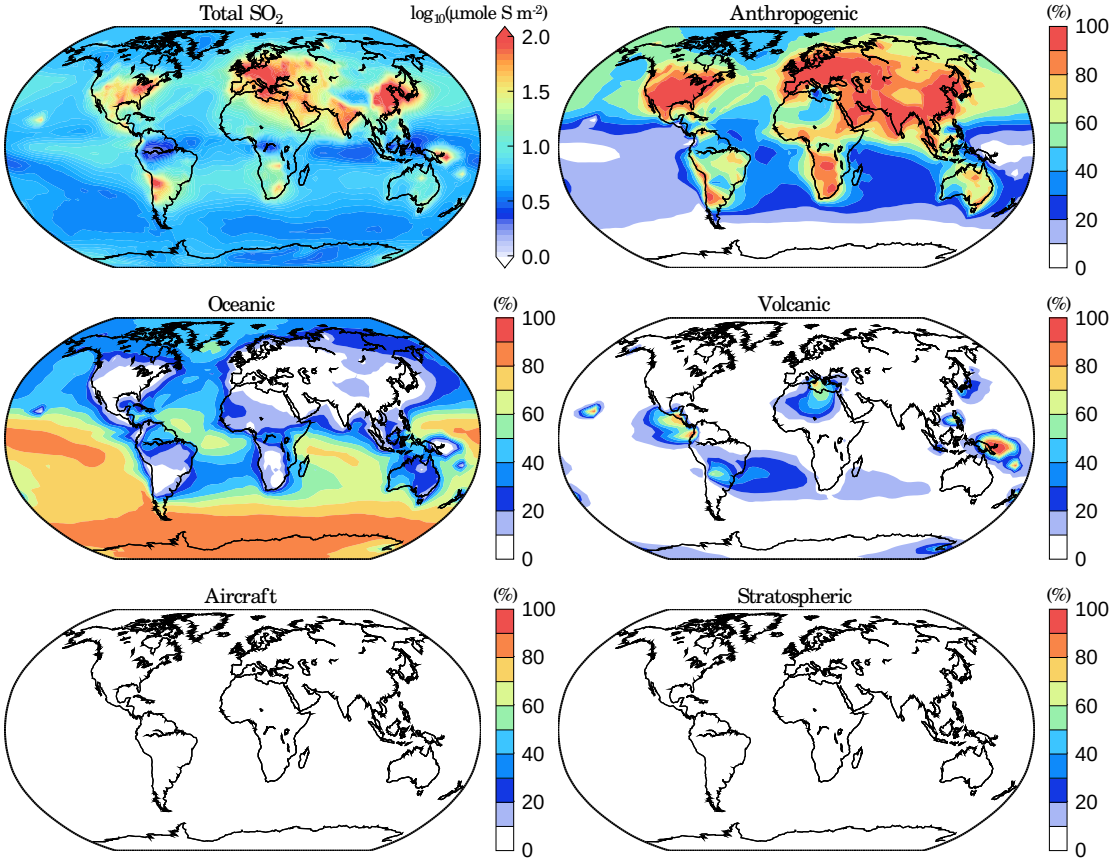

Fig. 3. Annual average column burdens of the total SO_2 from all of the sources (upper left panel) and the percent contributions of the tagged sources to the total SO_2 (other panels).

ACPD
7, 7679–7721, 2007

EGU

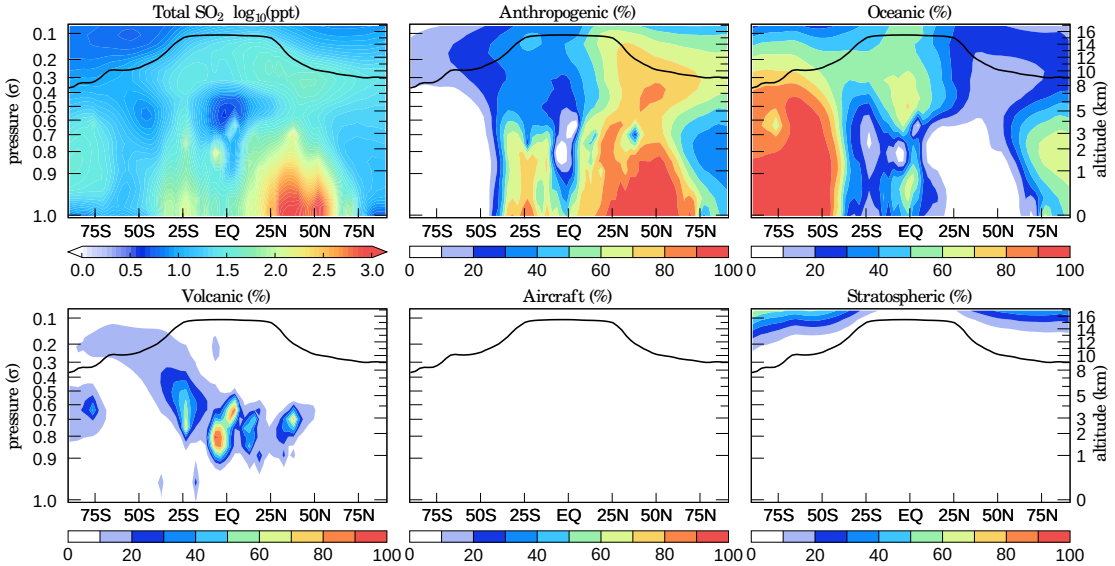

Fig. 4. Annual zonal average mole fractions of the total SO_2 from all of the sources (upper left panel) and the percent contributions of the tagged sources to the total SO_2 (other panels).

ACPD
7, 7679–7721, 2007

EGU

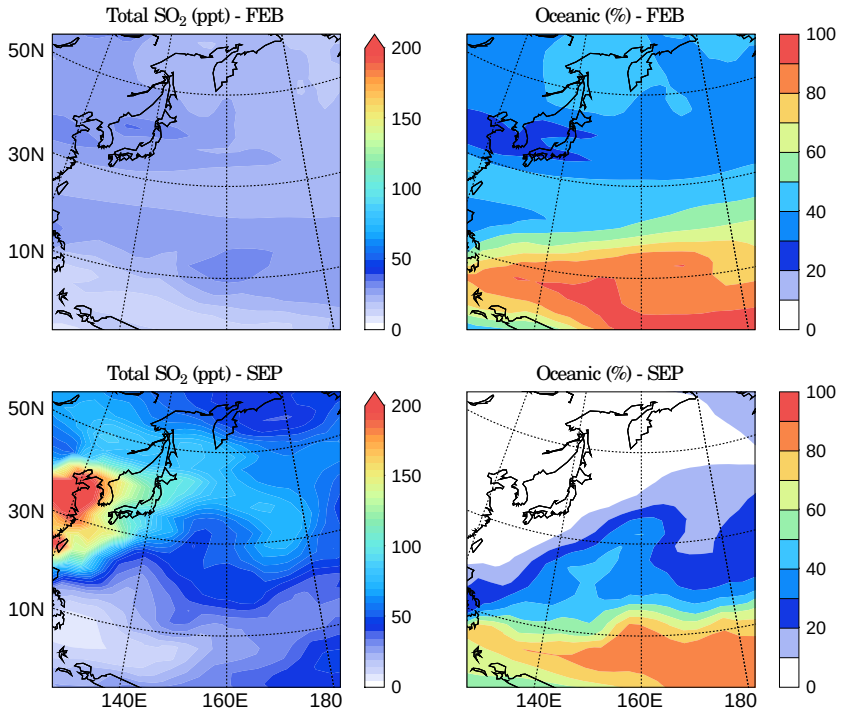

Fig. 5. Monthly average mole fractions of SO_2 (left panels, ppt) and the percent contributions from oceanic sulfur (right panels) at a high altitude level over the western Pacific for February (upper panels) and September (lower panels). The high altitude level corresponds to the approximate model level of 284–341 hPa.

ACPD
7, 7679–7721, 2007

EGU

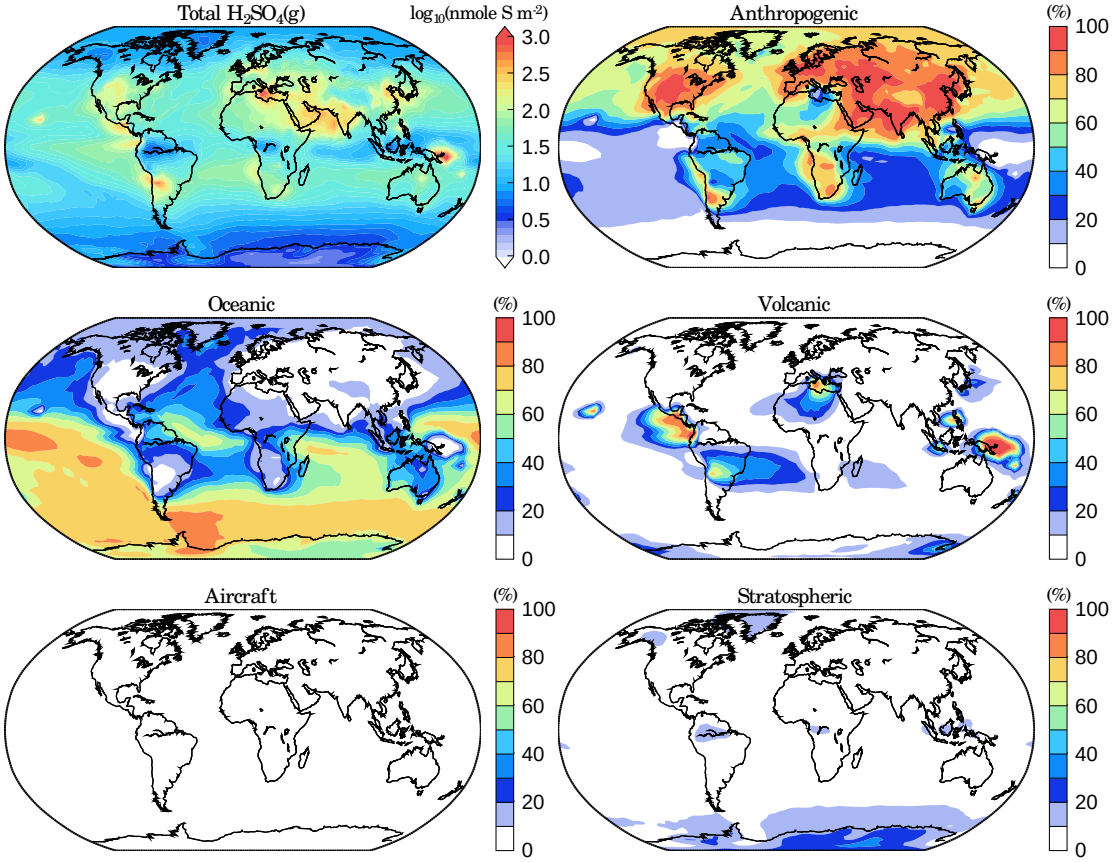

Fig. 6. Annual average column burdens of the total H_2SO_4(g) from all of the sources (upper left panel) and the percent contributions of the tagged sources to the total H_2SO_4(g) (other panels).

ACPD
7, 7679–7721, 2007

EGU

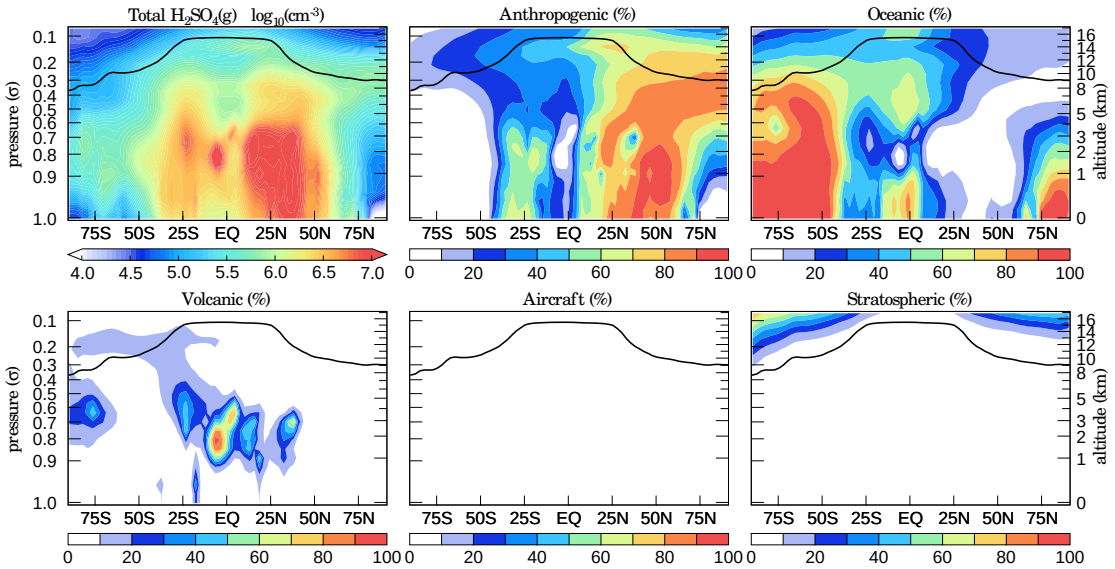

Fig. 7. Annual zonal average concentrations of the total H_2SO_4(g) from all of the sources (upper left panel) and the percent contributions of the tagged sources to the total H_2SO_4(g) (other panels).

ACPD
7, 7679–7721, 2007

EGU

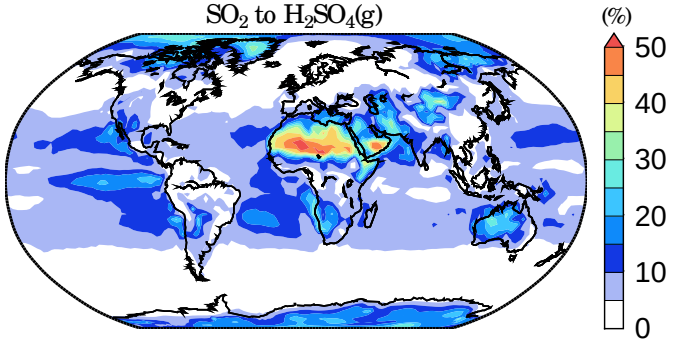

Fig. 8. SO_2 to H_2SO_4(g) conversion efficiency. The efficiency is calculated from the ratio of the annually averaged and vertically integrated gas-phase loss of SO_2 to the net loss of SO_2.

ACPD
7, 7679–7721, 2007

EGU

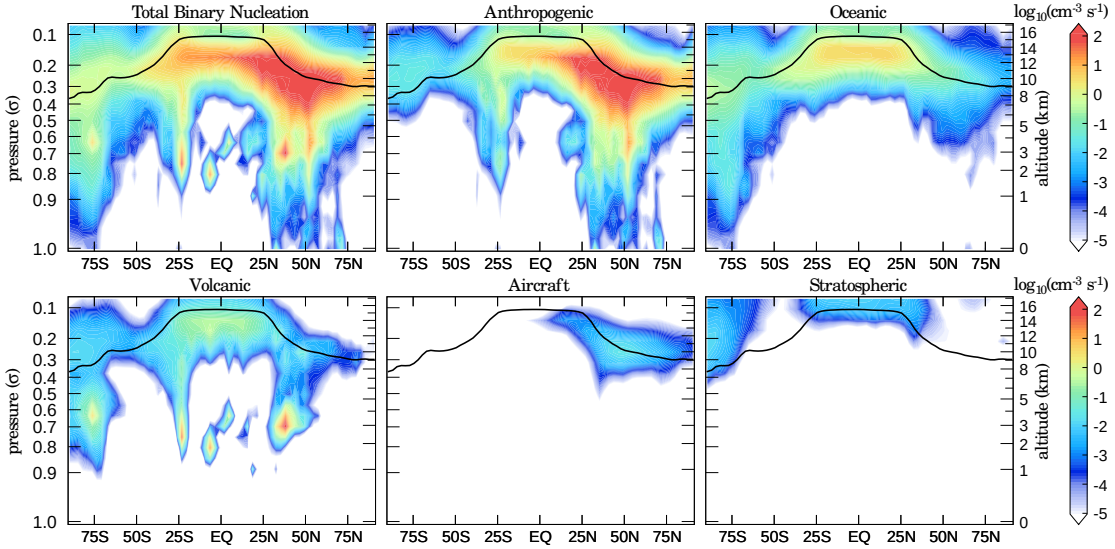

Fig. 9. Annual zonal average rates of forming nanoparticles by binary nucleation. NP formation rates using all of the sources (total binary nucleation) are shown in the upper left panel. The remaining panels show the rates using the tagged tracers.

ACPD
7, 7679–7721, 2007

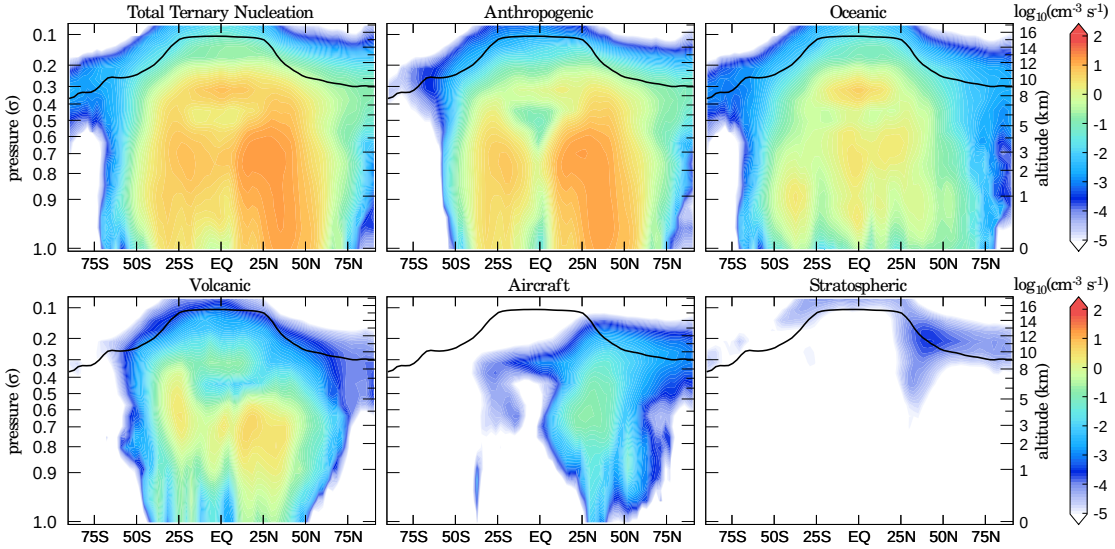

Fig. 10. Annual zonal average rates of forming nanoparticles by ternary nucleation. NP formation rates using all of the sources (total ternary nucleation) are shown in the upper left panel. The remaining panels show the rates using the tagged tracers.

ACPD
7, 7679–7721, 2007

EGU

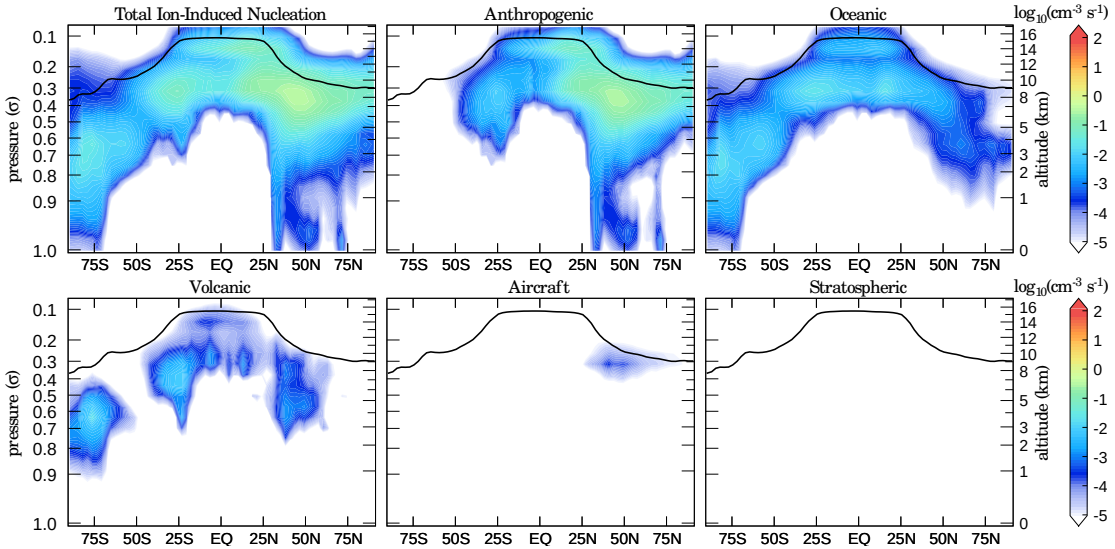

Fig. 11. Annual zonal average rates of forming nanoparticles by ion-induced nucleation. NP formation rates using all of the sources (total ion-induced nucleation) are shown in the upper left panel. The remaining panels show the rates using the tagged tracers.

ACPD
7, 7679–7721, 2007

EGU